Effect of electron localization on the edge-state spins in a disordered network of nanographene sheets

V. L. Joseph Joly, Katsunori Takahara, Kazuyuki Takai, Ko Sugihara, and Toshiaki Enoki*
Department of Chemistry, Tokyo Institute of Technology, 2-12-1 Ookayama, Meguro-ku, Tokyo 152-8551, Japan

Mikito Koshino and Hidekazu Tanaka
Department of Physics, Tokyo Institute of Technology, 2-12-1 Ookayama, Meguro-ku, Tokyo 152-8551, Japan
(Received 31 July 2009; revised manuscript received 27 January 2010; published 5 March 2010)

The magnetism and its dynamical behavior is investigated in relation to electron-localization effect for the edge-state spins of three-dimensional randomly networked nanographene sheets which interact weakly with each other. The electron transport is governed by Coulomb-gap variable-range hopping between nanographene sheets. At high temperatures, the electron spin resonance (ESR) signal with a feature of homogeneous spin system reveals the bottleneck effect in the spin relaxation to the lattice for a strongly coupled system of edge-state spins and conduction π electrons, in a given nanographene sheet. Below 20 K, a discontinuous ESR line broadening accompanied by hole-burning proves the formation of an inhomogeneous spin state, indicating a static spatial distribution of on-resonance fields. This inhomogeneity originates from a distribution of the strengths of the ferrimagnetic moments on the individual nanographene sheets, taking into account that the constituent nanographene sheets with their shapes randomly varying have different strengths of ferrimagnetic moments. Strong electron localization below 20 K in the internanographene electron hopping is responsible for the crossover from the homogeneous spin state to the inhomogeneous one, in the latter of which ferrimagnetic short-range ordering is evident in the edge-state spin system.

DOI: 10.1103/PhysRevB.81.115408 PACS number(s): 72.15.Rn, 75.30.Hx, 76.30.−v

I. INTRODUCTION

Graphene has attracted great attention in the research on carbon-based nanomaterials after the discovery of graphene prepared by micromechanical cleavage.[1–4] Current works on graphene have revealed unconventional electronic features such as unusual half-integer quantum Hall effect,[5] quantum spin-Hall effect,[6] quantum dots,[7] etc., for which its electronic structure described in terms of massless Dirac fermion is responsible. When the size of graphene sheet decreases to the nanodimension, another intriguing aspect emerges because of the growing importance of its geometrical shape. Indeed, nanographene, whose shape is described in terms of a combination of armchair and zigzag edges, has spin-polarized nonbonding π-electron state (edge-state) localized in the zigzag-edge region in spite of the absence of such state in armchair edges, as suggested by theoretical predictions,[8,9] and scanning tunneling microscope/scanning tunneling spectroscopy (STS) experiments.[10–14] The presence of edge-state spins therefore results in a variety of magnetism in nanographene, depending on its shape.

According to theoretical studies,[15–18] the edge-state spins are strongly coupled in parallel with each other in a zigzag edge through strong intrazigzag-edge ferromagnetic interaction J_0 having a strength of $\sim 10^3$ K, as shown in Fig. 1. In a nanographene sheet with zigzag-edge regions separated by the presence of armchair edges, the ferromagnetically coupled edge-state spins in a zigzag edge are interacting with those in other zigzag edge through interzigzag-edge ferromagnetic/antiferromagnetic interaction J_1 having a strength of $\sim(10^{-1}-10^{-2})J_0$ and mediated by conduction π carriers, where the strength and sign of J_1 depend on the mutual structural relation between the zigzag edges. Then, the cooperation of strong ferromagnetic interaction J_0 and intermediate-strength ferromagnetic/antiferromagnetic interaction J_1 plays an important role in the magnetism of a nanographene sheet. Here, the localized edge-state spins and conduction π carriers are the players similar to the *d*-electron spins and conduction *s* carriers in traditional *s-d* electronic systems.[19–21] Interestingly, an arbitrary-shaped nanographene sheet, whose periphery is constituted with ferromagnetic zigzag edges embedded between nonmagnetic armchair edges, is expected to have a ferrimagnetic structure; that is, a nonzero net ferrimagnetic moment can originate from a compensation of the constituent spins coupled by J_0 and J_1, as modeled in Fig. 1. In addition, the negligible magnetic anisotropy associated with a small spin-orbit interaction of carbon[22]

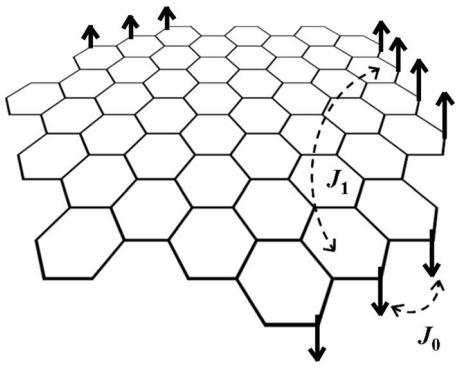

FIG. 1. Model structure of an arbitrary-shaped nanographene sheet, which consists of a combination of zigzag and armchair edges, the former of which has localized spins of edge-state ferromagnetically arranged. J_0 and J_1 are the intrazigzag-edge ferromagnetic and interzigzag-edge ferromagnetic/antiferromagnetic exchange interactions, respectively.

gives a feature of isotropic Heisenberg spins.

However, no experimental effort has confirmed this theoretical conjecture. In other words, experimental evidence is particularly important for this conjecture on the ferrimagnetic feature.

In the mean time, activated carbon fiber (ACF) arises as an interesting model system in order to investigate the magnetism of nanographene experimentally.[23–27] It consists of a three-dimensional (3D) disordered network of nanographite domains, each of which is a loose stack of 3–4 nanographene sheets with a mean in-plane size of 2–3 nm.[28] Here, two kinds of extra interactions should be added due to its hierarchical structure; weak internanographene-sheet antiferromagnetic interaction J_2, and internanographite-domain antiferromagnetic one J_3. J_3 originates from the internanographite-domain hopping integral and is in the range of several kelvins.[23] Since the electron transport in nanographene network is governed by the Coulomb-gap-type variable-range hopping,[24,29] strong electron localization is expected at lower temperatures, which in turn can affect the magnetism. Therefore, the magnetism and its dynamical behavior of the edge-state spin system in the nanographene network are of particular interest in relation to the electron-localization phenomenon. In this paper, we show the electron-localization-induced inhomogeneous magnetic state of the edge-state spins in the networked nanographene sheets, which are weakly coupled with each other, from the results of electron spin resonance (ESR), static magnetic susceptibility, and electrical conductivity experiments in vacuum and oxygen atmosphere with carefully prepared ACF samples. The experimental findings unveiled the ferrimagnetic structure of nanographene sheet as a fingerprint of the edge-state spins, which has also been evident in the magnetic susceptibility of the samples specially treated.[30]

II. EXPERIMENTAL

Phenol-based ACFs (FR-20, Kuraray Chemicals) having specific surface areas of ~2000 m^2/g were preheat treated at 473 K for 12 h in vacuum (10^{-5} Pa) to remove the adsorbed foreign gas species. We have introduced controlled amounts of high-purity O_2 (99.99995 %) up to 20 Pa at room temperature after the preheat treatment, to investigate the effect of adsorbed O_2 molecules on the magnetism. X-band ESR measurements were carried out in heating runs at 4–300 K in the microwave-power range up to 16 mW using JEOL TE-200 X-band ESR spectrometer equipped with Oxford ESR910 helium continuous-flow cryostat. The bundled sample (~1 mg) was sealed in a quartz tube in vacuum or in the oxygen atmosphere. In order to avoid surface skin depth effect, the fiber axes of the bundle were oriented perpendicular to the electric field direction of the microwave. The static susceptibility was measured in the temperature range 2–300 K at 1 T using superconducting quantum interference device magnetometer (Quantum Design MPMS-5). The resistivity was measured using two-probe method with a single ACF fiber (approximately 10 μm in diameter) in vacuum at 2–300 K. Carbon paste was used to make electrical contacts to the electrodes.

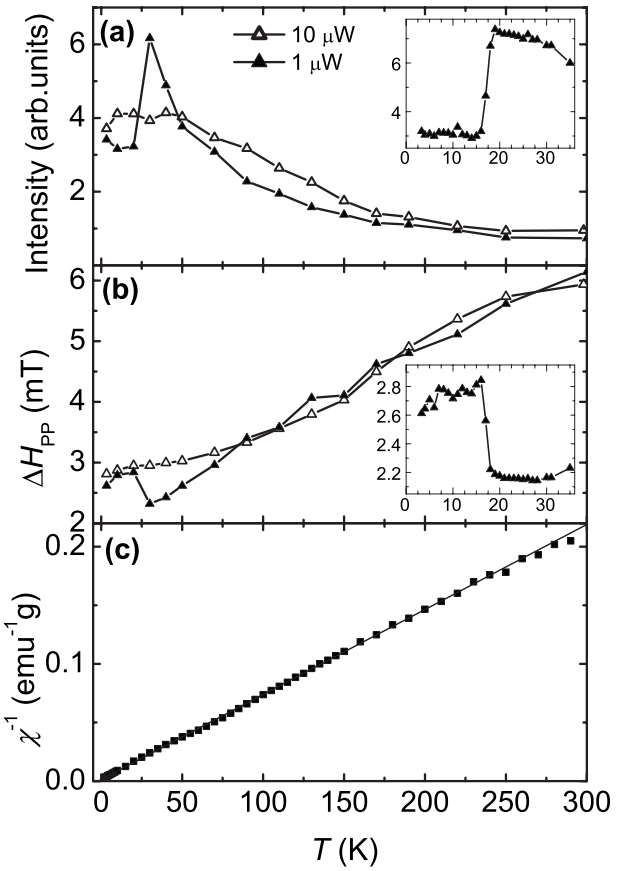

FIG. 2. (a) Temperature dependence of ESR intensity in vacuum, at 1 μW (▲) and 10 μW (△) microwave power. (b) The corresponding peak-to-peak widths ΔH_{PP} of the ESR signal obtained after fitting the Lorentzian function. Insets of (a) and (b): zoomed-in curves in the range 4–35 K for 1 μW. (c) Inverse static susceptibility as a function of temperature in vacuum (■) and the linear fit (solid line), measured at $H=1$ T.

III. RESULTS

The temperature dependence of the ESR intensity and peak-to-peak width (ΔH_{PP}) in vacuum, at microwave powers of 1 and 10 μW are given in Figs. 2(a) and 2(b), respectively. The intensity at 1 μW obeys the Curie law down to 30 K, and suddenly drops by 50 % below 20 K. ΔH_{PP} follows a trend corresponding to the behavior of the intensity. ΔH_{PP} decreases linearly from 6.2 to 2.2 mT upon lowering of the temperature down to 30 K, and suddenly increases by 30% (0.6 mT) below 20 K. In the elevated microwave power (10 μW), the sudden change in the signal properties becomes a smooth variation as shown in Figs. 2(a) and 2(b). Such sensitive nature of the ESR signal below 20 K is also evident in the microwave-power dependence of the intensity as shown in Fig. 3. The power saturation at 30 K has a feature of a homogeneous spin system. On the other hand, at 10 K, increasing the power above 200 μW doubles the intensity suddenly and then it is easily saturated in the higher microwave-power range above 1 mW, showing inhomogeneity in the spin system. Unlike the ESR intensity that represents the dynamical susceptibility, the static susceptibility, which corresponds to the susceptibility at frequency $\omega=0$,

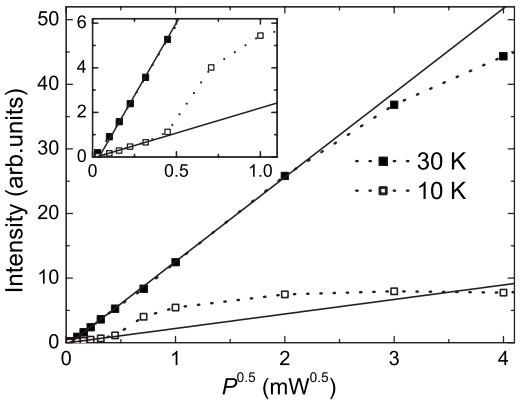

FIG. 3. Microwave-power dependence of ESR intensity in vacuum, at 30 K (■) and 10 K (□). The blown-up view of low-power region is given in the inset. The solid lines are straight-line fit to the low-power region and dashed lines are guide to the eyes.

does not show any indications of non-Curie behavior down to 2 K as shown in Fig. 2(c). Indeed, the static susceptibility obeys the Curie-Weiss law in the entire temperature range with a small negative Weiss temperature of −2 to −3 K for which J_3 is responsible as a major contribution.[23,24] These experimental findings are therefore understood by the presence of a transition from the homogeneous state to an inhomogeneous one at approximately 20 K. This is clearly evident in observing a change in the line profile in the vicinity of the transition temperature ($T_c \sim 20$ K). Figure 4 exhibits the ESR signal at a strong microwave power of 16 mW in the vicinity of T_c. The broadened signal at 10 K shows a slight deviation from the Lorentzian shape indicating an inhomogeneous line broadening. A prominent hole-burning effect (irregular feature in the ESR signal) appears at 15 K, which is just below T_c, and it is reproducible in repeated runs. The hole-burning feature is an important evidence of serious inhomogeneity appearing in this temperature range. On going to higher temperatures, hole burning is gradually suppressed and the line shape tends to become Lorentzian. Above 25 K, the line shape becomes sharpened and purely Lorentzian, exchange/motional narrowing being indicated.

The feature of the ESR signal is extremely sensitive to the presence of O_2 molecules, even though the amount of adsorbed oxygen is considerably low. Figure 5 shows the oxygen adsorption effect on the ESR spectra in the O_2 pressure up to 20 Pa. The transition temperature T_c, at which the intensity is peaked, is shifted to higher temperature and the change in ΔH_{PP} at T_c is reduced in proportion to the O_2 pressure. Eventually above 1 Pa, the transition behavior is leveled off. The limit of shift in the T_c is 100 K, where the physisorption of magnetic O_2 molecules takes place.[27]

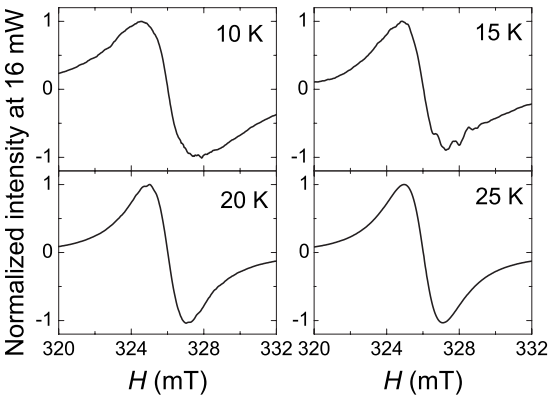

FIG. 4. The ESR signals in vacuum at 10, 15, 20, and 25 K measured with 16 mW.

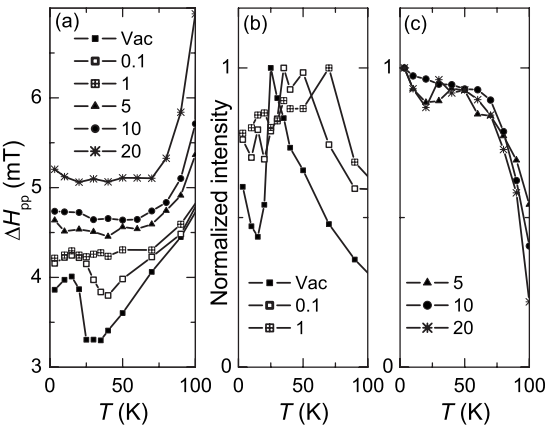

FIG. 5. (a) Temperature dependence of ESR peak-to-peak widths in vacuum (■) and oxygen pressures of 0.1 Pa (□), 1 Pa (⊞), 5 Pa (▲), 10 Pa (●), and 20 Pa (∗). Oxygen was introduced at room temperature, before cooling. (b) and (c) The corresponding normalized signal intensities.

Figure 6(a) shows the temperature dependence of conductivity. The conductivity is explained in terms of the Coulomb-gap variable-range hopping (CVRH) transport between randomly distributed metallic nanographene sheets,[24,29]

$$\sigma(T) = \sigma_0 \exp[-(T_0/T)^{\gamma}], \tag{1}$$

where σ_0 is the conductivity at $T=\infty$ and T_0 is a function of localization length, L. In the conventional CVRH behavior,[31] the exponent $\gamma=0.5$ is expected even in three-dimensional Anderson insulators. However, the present experimental results in Fig. 6(a) deviates from that expected and is best fitted with an estimate of $\gamma=0.57$ as shown in Fig. 6(b), suggesting the importance of fractal geometry of the nanographene network.[32,33] Here localization length L is given by the following relation:[34]

$$L = \frac{e^2}{4\pi\epsilon_0\epsilon_r k_B T_0} \frac{(1-\gamma)^{1-1/\gamma}}{\gamma}, \tag{2}$$

where ϵ_r and ϵ_0 are the relative permittivity of ACFs and the dielectric constant of vacuum, respectively. With $T_0 = 324$ K obtained from the linear fit of the experimental results shown in Fig. 6(b), L is obtained as ~17 nm, using the value of $\epsilon_r=10$ for amorphous carbon.[24] This satisfies the criteria for VRH on fractal, i.e., $T<T_0$ and $a<L$, (average size of nanographene sheet; $a=2-3$ nm). In other words, the electron transport is subjected to the fractal structure of the nanographene network.

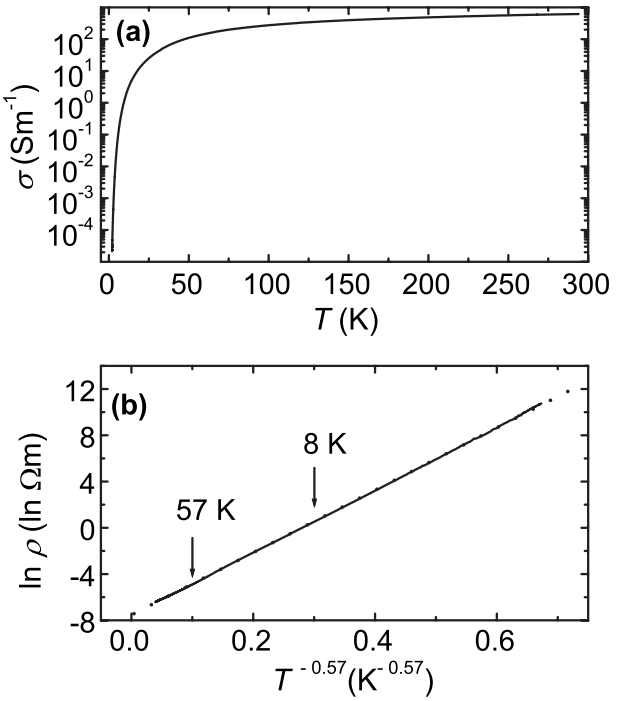

FIG. 6. (a) Temperature dependence of dc conductivity in vacuum. (b) Resistivity vs temperature plot corresponding to (a) and linear fit (dotted line). The arrow marks correspond to 57 and 8 K.

IV. DISCUSSION

Let us discuss the magnetic structure and dynamics underlying the observed magnetic and transport properties. The conductivity result suggests strong electron localization with the aid of Coulomb interaction, particularly in the lower temperature region. In addition to the electron hopping in the 3D random network of metallic nanographene sheets, the π-electron carriers interact with the edge-state localized spins of a given sheet. At high temperatures, the fast hopping process evidenced by the high conductivity makes the edge-state spins subjected to the motional narrowing, yielding a homogeneous spin system in the entire of the network. This is justified by the Lorentzian shape of the ESR signal and its less saturated behavior (see Fig. 3) in the high-temperature range. Therefore, the spin system is modeled merely as a metallic system with the interaction between the localized edge-state spins and conduction π carriers. This is reminiscent of traditional *s-d* dilute alloy magnetic systems such as CuMn,[21] if we take π-conduction electrons and edge-state spins in place of *s* carriers and localized *d*-electron spins, respectively. Here, the strong coupling between the edge-state spins and conduction π carriers, and weak spin-orbit interaction,[22] leads to a bottleneck in energy dissipation from the conduction carriers to the lattice. (A considerably small deviation of the *g* value from that of the free-electron spin ($\Delta g = 10^{-3}$) proves the very small spin-orbit interaction in this system, in good agreement with that in element C (~ 5 cm^{-1})) In this regime, the effective spin-lattice relaxation time, which is inversely proportional to the linewidth, is given as[20,35]

$$\Delta H \sim 1/T_{1eff} = 1/T_{n\pi}(T_{\pi n}/T_{\pi \mathrm{L}}), \tag{3}$$

where, $T_{n\pi}$, $T_{\pi n}$, and $T_{\pi \mathrm{L}}$ are the relaxation times of from the edge-state spin to the π carrier, from the π carrier to the edge-state spin, and from the π carrier to the lattice, respectively. The relaxation from the edge-state spins to the π carriers, $T_{n\pi}$ is given by the Korringa relation with temperature dependence of $T_{n\pi} \propto 1/T$.[36]

Then, as shown in Eq. (3), the linewidth is narrowed by $(T_{\pi n}/T_{\pi \mathrm{L}})$ due to the bottleneck effect with a slow relaxation rate $1/T_{\pi \mathrm{L}}$ (long relaxation time). Here, it should be noted that $T_{\pi n}$ is independent of temperature[20] and $T_{\pi \mathrm{L}}$, which is governed by the boundary scattering in the nanographene is also less temperature dependent.[37] In other words, the temperature dependence in the linewidth is governed by the Korringa relation. Eventually, the linear temperature dependence of the linewidth observed above $T_c \sim 20$ K [Fig. 2(b)] is in good agreement with that expected by Eq. (3). This suggests the importance of the interplay between the edge-state spins and conduction π carriers strongly interacting with each other in the metallic medium.

The explanation of the inhomogeneous behavior below $T_c \sim 20$ K with a discontinuous change in the ESR signal requires detailed information on the magnetic structure of the nanographene network. In conventional cases, the inhomogeneous broadening is associated with the dipolar interaction. However, in those cases, the application of high microwave power deforms mainly the central part of the ESR signal instead of the appearance of irregular features of hole-burning observed in the present experiment. The appearance of hole-burning phenomenon is instead a consequence of the presence of a static distribution of on-resonance fields, which indicates the importance of the structural inhomogeneity. Accordingly, we should examine an alternative origin of the inhomogeneity on the basis of the structural feature of the nanographene network.

Here is a clue in the structure of constituent nanographene sheet in order to solve this issue. Indeed, as explained in Sec. I with Fig. 1, each nanographene sheet has its own shape, consisting of arbitrarily positioned zigzag and armchair edges. In an individual nanographene sheet, the compensation of randomly distributed localized spins coupled by ferromagnetic J_0 and ferromagnetic/antiferromagnetic J_1 creates a nonzero net magnetic moment with its own strength. Therefore, the strengths of the ferrimagnetic magnetic moments, which depend on the shape of a nanographene sheet, are randomly distributed in the network of nanographene sheets. This suggests that the on-resonance fields vary inhomogeneously in the ESR signal, depending on the strengths of the magnetic moments of nanographene sheets. The inhomogeneity associated with the distribution of on-resonance fields does not appear in the high-temperature range due to the motional narrowing operated by the fast internanographene-sheet hopping. However, as the temperature is lowered, electron localization develops and nanographene sheets become independent from each other due to the slowdown of electron hopping. Finally, the inhomogeneity survives at lower temperatures below $T_c \sim 20$ K, where the electron hopping frequency becomes

small enough to unveil the inhomogeneous linewidth, $\Delta H_{\mathrm{inhom}} \simeq \Delta H(T<T_c) - \Delta H(T>T_c) \sim 0.6$ mT. Looking at the experimental finding from another perspective, the observed inhomogeneity reveals a ferrimagnetic feature of individual nanographene sheet as exhibited in Fig. 1, which is predicted from theoretical work.[15–18] Recent work on magnetic investigations of the ACF samples, in which the internanographene-sheet interaction J_2 is weakened by acid treatment, proves the presence of ferrimagnetic spin fluctuations[30] in good agreement with the present finding, though the apparent Curie-type behavior appears in the present sample due to the presence of weak internanographene-sheet interaction and the absence of magnetic anisotropy as shown in Fig. 2(c).

Interestingly, in relation to the inhomogeneous magnetic state, we remind that a spin-glass state is created in the vicinity of an insulator-to-metal transition in the networked nanographene sheets of the ACF sample.[23] In the ACF sample, heat treated below 473 K, the presence of oxygen-including functional groups bonded to edge carbon atoms, which work to block the carriers to hop by weakening the internanographene-sheet interaction,[38] results in the formation of an Anderson insulator. Heat treatment above ~1273 K, which can remove the functional groups, enhances the interaction, and further increase in the heat-treatment temperature brings about an insulator-to-metal transition around 1473 K. The spin-glass state of the edge-state spins appears in the vicinity of the insulator-to-metal transition.[23] According to the present results, it is considered that the strengthening of the internanographene-sheet interaction induced by the heat treatment brings the inhomogeneous assembly of relatively independent ferrimagnetic nanographene sheets to a spin-glass state in the vicinity of the transition. Then, further strengthening of the interaction well above the transition temperature works to form metallic state at the expense of the edge-state spins.

Finally, we discuss the oxygen adsorption effect, which is summarized as the increase in the linewidth and the disappearance of the linewidth anomaly under the presence of a slight amount of O_2 molecules (<1 Pa). According to previous works in the small oxygen concentration range, the majority of the oxygen species are chemisorbed and become nonmagnetic due to charge transfer from nanographene sheets.[27,38–40] Chemisorbed O_2 molecules randomly bonded to the nanographene edges inhomogeneously downshift the Fermi energies of constituent nanographene sheets, resulting in enhancing the charge inhomogeneity in the network. This works to upshift the transition temperature to the inhomogeneous magnetic state as shown in Fig. 5 due to enhanced charge localization. This is also in good agreement with the decrease in the conductivity upon the oxygen uptake.[38] Under higher O_2 pressure (>5 Pa), the dipolar field of physisorbed magnetic O_2 molecules broadens the ESR linewidth as observed in Fig. 5(a).

V. SUMMARY

In summary, the magnetism and electron transport are investigated for randomly networked nanographene sheets which interact weakly with each other. The transport is governed by Coulomb-gap-type variable-range hopping on a fractal network. At high temperatures, the edge-state spins of an individual nanographene sheet is subjected to the bottleneck effect in the strongly coupled system of the edge-state spins and conduction π carriers. Below 20 K, the electron localization unveils the inhomogeneous distribution of ferrimagnetic structures of nanographene sheets, each of which has its own magnetic moment depending on its geometrical shape. The present experiment demonstrates the ferrimagnetic fluctuations of the edge-state spins of nanographene sheet.

ACKNOWLEDGMENTS

The present work is supported by the Grant-in-Aid for Scientific Research No. 20001006 from the Ministry of Education, Culture, Sports, Science and Technology, Japan.

*enoki.t.aa@m.titech.ac.jp

[1] K. S. Novoselov, A. K. Geim, S. V. Morozov, D. Jiang, Y. Zhang, S. V. Dubonos, I. V. Grigorieva, and A. A. Firsov, Science **306**, 666 (2004).
[2] C. Berger, Z. Song, T. Li, X. Li, A. Y. Ogbazghi, R. Feng, Z. Dai, A. N. Marchenkov, E. H. Conrad, P. N. First, and W. A. de Heer, J. Chem. Phys. B **108**, 19912 (2004).
[3] V. V. Cheianov, V. Fal'ko, and B. L. Altshuler, Science **315**, 1252 (2007).
[4] A. H. Castro Neto, F. Guinea, N. M. R. Peres, K. S. Novoselov, and A. K. Geim, Rev. Mod. Phys. **81**, 109 (2009).
[5] Y. Zhang, Y. Tan, H. L. Stormer, and P. Kim, Nature (London) **438**, 201 (2005).
[6] C. L. Kane and E. J. Mele, Phys. Rev. Lett. **95**, 226801 (2005).
[7] B. Trauzettel, D. V. Bulaev, D. Loss, and G. Burkard, Nat. Phys. **3**, 192 (2007).
[8] M. Fujita, K. Wakabayashi, K. Nakada, and K. Kusakabe, J. Phys. Soc. Jpn. **65**, 1920 (1996).
[9] K. Nakada, M. Fujita, G. Dresselhaus, and M. S. Dresselhaus, Phys. Rev. B **54**, 17954 (1996).
[10] Y. Kobayashi, K. I. Fukui, T. Enoki, K. Kusakabe, and Y. Kaburagi, Phys. Rev. B **71**, 193406 (2005).
[11] Y. Kobayashi, K. I. Fukui, T. Enoki, and K. Kusakabe, Phys. Rev. B **73**, 125415 (2006).
[12] Y. Niimi, T. Matsui, H. Kambara, K. Tagami, M. Tsukada, and H. Fukuyama, Phys. Rev. B **73**, 085421 (2006).
[13] T. Enoki, Y. Kobayashi, and K. Fukui, Int. Rev. Phys. Chem. **26**, 609 (2007).
[14] T. Enoki and K. Takai, Solid State Commun. **149**, 1144 (2009).
[15] K. Wakabayashi, M. Sigrist, and M. Fujita, J. Phys. Soc. Jpn. **67**, 2089 (1998).
[16] J. Inoue, K. Fukui, T. Kubo, S. Nakazawa, K. Sato, D. Shiomi,

Y. Morita, K. Yamamoto, T. Takui, and K. Nakasuji, J. Am. Chem. Soc. **123**, 12702 (2001).
[17] K. Nakasuji and T. Kubo, Bull. Chem. Soc. Jpn. **77**, 1791 (2004).
[18] Y.-W. Son, M. L. Cohen, and S. G. Louie, Nature (London) **444**, 347 (2006).
[19] J. Owen, M. Browne, W. D. Knight, and C. Kittel, Phys. Rev. **102**, 1501 (1956).
[20] H. Hasegawa, Prog. Theor. Phys. **21**, 483 (1959).
[21] R. H. Taylor, Adv. Phys. **24**, 681 (1975).
[22] K. Matsubara, T. Tsuzuku, and K. Sugihara, Phys. Rev. B **44**, 11845 (1991).
[23] Y. Shibayama, H. Sato, T. Enoki, and M. Endo, Phys. Rev. Lett. **84**, 1744 (2000).
[24] Y. Shibayama, H. Sato, T. Enoki, X. Xin Bi, M. S. Dresselhaus, and M. Endo, J. Phys. Soc. Jpn. **69**, 754 (2000).
[25] K. Takai, H. Sato, T. Enoki, N. Yoshida, F. Okino, H. Touhara, and M. Endo, J. Phys. Soc. Jpn. **70**, 175 (2001).
[26] H. Sato, N. Kawatsu, T. Enoki, M. Endo, R. Kobori, S. Maruyama, and K. Kaneko, Solid State Commun. **125**, 641 (2003).
[27] V. L. Joseph Joly, K. Takai, and T. Enoki, J. Phys. Chem. Solids (to be published).
[28] K. Kaneko, C. Ishii, M. Ruike, and H. kuwabara, Carbon **30**, 1075 (1992).
[29] A. W. P. Fung, Z. H. Wang, M. S. Dresselhaus, G. Dresselhaus, R. W. Pekala, and M. Endo, Phys. Rev. B **49**, 17325 (1994).
[30] S. Tsuge, K. Nakajima, M. Hara, K. Takai, and T. Enoki (private communication).
[31] A. L. Efros and B. I. Shklovskii, J. Phys. C **8**, L49 (1975).
[32] A. Aharony and A. B. Harris, Physica A **163**, 38 (1990).
[33] A. Aharony, O. Entin-Wohlman, and A. B. Harris, Physica A **200**, 171 (1993).
[34] D. van der Putten, J. T. Moonen, H. B. Brom, J. C. M. Brokken-Zijp, and M. A. J. Michels, Phys. Rev. Lett. **69**, 494 (1992).
[35] J. H. Pifer and R. T. Longo, Phys. Rev. B **4**, 3797 (1971).
[36] J. Korringa, Physica **16**, 601 (1950).
[37] O. E. Andersson, B. L. V. Prasad, H. Sato, T. Enoki, Y. Hishiyama, Y. Kaburagi, M. Yoshikawa, and S. Bandow, Phys. Rev. B **58**, 16387 (1998).
[38] G. U. Sumanasekera, G. Chen, K. Takai, J. Joly, N. Kobayashi, T. Enoki, and P. C. Eklund, J. Phys.: Condens. Matter (to be published).
[39] N. Kobayashi, T. Enoki, Y. Murakami, H. Suematsu, and M. Endo, Mol. Cryst. Liq. Cryst. **306**, 103 (1997).
[40] N. Kobayashi, T. Enoki, C. Ishii, K. Kaneko, and M. Endo, J. Chem. Phys. **109**, 1983 (1998).